Journal of the Mechanics and Physics of Solids 60 (2012) 451–470

Contents lists available at SciVerse ScienceDirect

Journal of the Mechanics and Physics of Solids

journal homepage: www.elsevier.com/locate/jmps

Generating virtual textile composite specimens using statistical data from micro-computed tomography: 1D tow representations for the Binary Model

Matthew Blacklock [a], Hrishikesh Bale [b], Matthew Begley [a], Brian Cox [c,*]

[a] University of California, Santa Barbara, CA, USA
[b] University of California, Berkeley, CA, USA
[c] Teledyne Scientific Co. LLC, Thousand Oaks, CA, USA

ARTICLE INFO

Article history:
Received 4 February 2011
Received in revised form
23 November 2011
Accepted 25 November 2011
Available online 8 December 2011

Keywords:
Textile composite
Stochastic microstructure
Virtual specimen
Geometry generator
Reconstruction algorithm

ABSTRACT

A Monte Carlo algorithm is defined for generating replicas of textile composite specimens that possess the same statistical characteristics as specimens imaged using high resolution computed tomography. The textile reinforcement is represented by one-dimensional tow loci in three-dimensional space, which are easily incorporated into the Binary Model of textile composites. A tow locus is expressed as the sum of non-stochastic, periodic variations in the coordinates of the tow centroid and stochastic, non-periodic deviations. The non-stochastic variations have period commensurate with the dimensions of the unit cell of the textile, while the stochastic deviations, which describe geometrical defects, exhibit correlation lengths that may be incommensurate with the unit cell. The model is calibrated with data deduced in prior work from computed tomography images. The calibration obviates the need for assuming any ideal shape functions for the tow loci, which can take very general form. The approach is therefore valid for a wide range of textile architectures. Once calibrated, a Markov Chain algorithm can generate numerous stochastic replicas of a textile architecture very rapidly. These virtual specimens can be much larger than the real specimens from which the data were originally gathered, a necessary feature when real specimen size is limited by the nature of high resolution computed tomography. The virtual specimen generator is illustrated using data for an angle interlock weave.

© 2011 Elsevier Ltd. All rights reserved.

1. Introduction

Numerous efforts are under way to establish Virtual Tests as engineering tools to aid materials design and reduce the number of physical tests required to certify a material for service. Several groups have recognized that an effective Virtual Test system must embrace both simulations and experiments to achieve a useful level of fidelity (Cox, 1989; Ashby, 1992; Cox and Yang, 2006; Cox et al., 2008; Pollock et al., 2008; Jiao et al., 2009). One key step is the use of experimental data to characterize the microstructure of the material in as much detail as necessary to allow realistic prediction of damage mechanisms that depend on certain microstructural features (Fig. 1). In many cases, the germane microstructural features are stochastic. To realize a Virtual Test cycle, not only must the statistics of the microstructure be characterized using

* Corresponding author.
E-mail address: brian1cox@yahoo.com (B. Cox).

0022-5096/$ - see front matter © 2011 Elsevier Ltd. All rights reserved.
doi:10.1016/j.jmps.2011.11.010

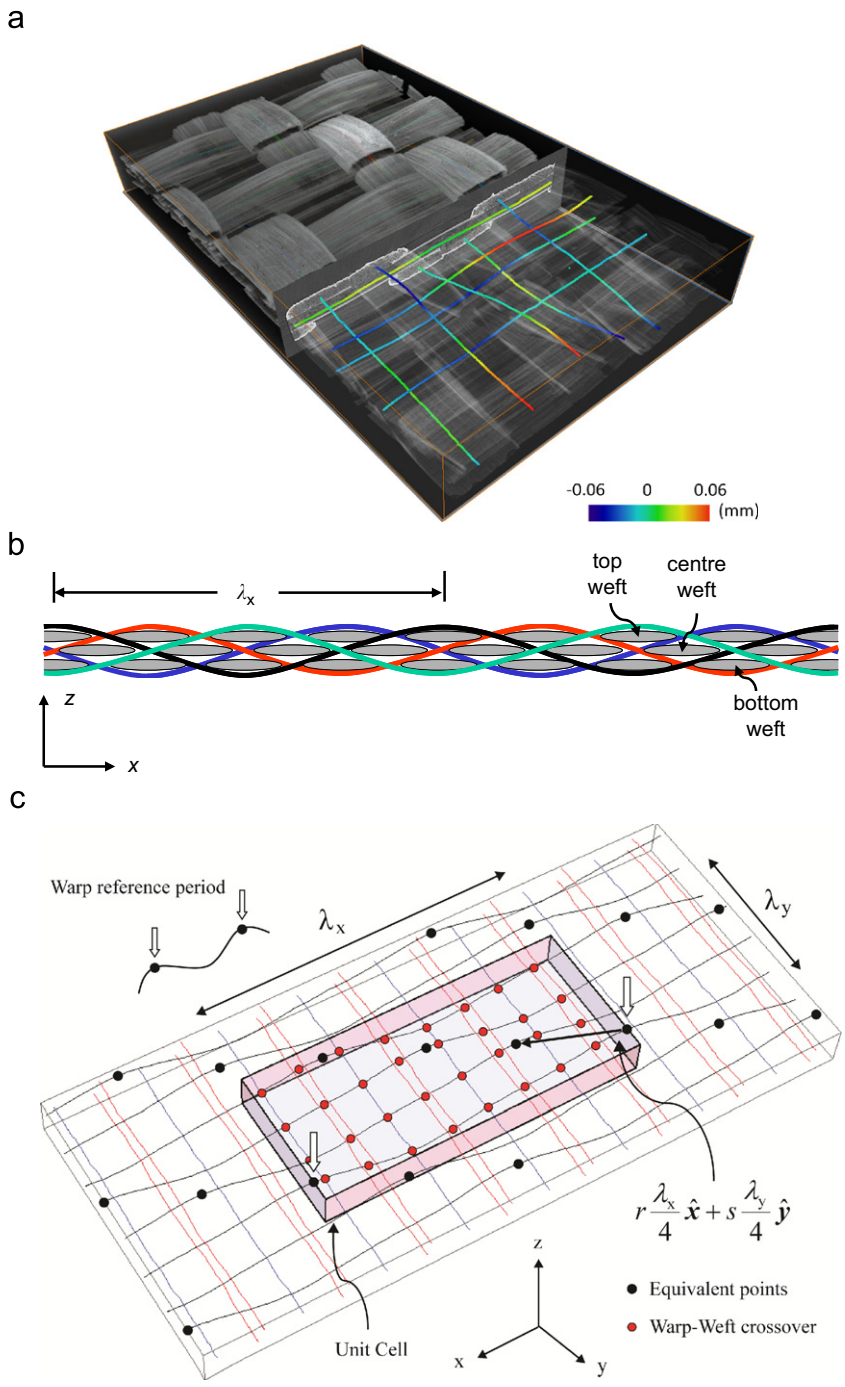

Fig. 1. Subject three-layer angle interlock architecture. (a) Image from μCT analysis of a C/SiC woven composite. Tow loci shown in the right portion of the image are the centers-of-mass of tow sections determined by analyzing image slices. The color code indicates the magnitude of deviations of the z-coordinate of a tow locus from an average locus for the tow genus (see text). (b) Schematic illustrating a section along the warp direction (the (x, z) plane), where warp tows appear as continuous curves and weft tows in section (ellipses). (c) 3D plot of tow loci, indicating the pattern of cross-overs within a single unit cell (smaller circles). One unit cell is marked in the (x, y) plane. The large circles on the warp tows are equivalent, in the periodic average structure, to each of the other points on warp tows that are marked by large circles. (For interpretation of the references to color in this figure legend, the reader is referred to the web version of this article.)

images of real specimens, but a "virtual specimen generator" must be formulated to create large numbers of replicas of the microstructure with the same statistics. The replicas serve as virtual specimens in simulations of damage evolution that can reveal the correlation between microstructural variations and material performance.

In the particular case of textile composites, one key microstructural characteristic is the spatial distribution of fiber tows. A recent article described the use of synchrotron-based high resolution computer tomography to map out fiber tows in a carbon fiber preform that had been rigidified by a coating of ceramic matrix deposited mainly on the tow surfaces (Bale et al., in press). The raw images were analyzed to identify the loci of the axes of all tows, along with variations in their cross-sectional area and shape, and the orientation of their cross-sections, throughout the volume covered by the image. The data can be used to calibrate a virtual specimen generator, which can create statistically faithful replicas of the imaged specimens.

In this first development of a virtual specimen generator, attention is restricted to the tow axes or centroids, which consist of a system of one-dimensional loci in three-dimensional space. The tow centroid loci are the necessary input for constructing Binary Model simulations of textile composite performance (Cox et al., 1994; Xu et al., 1995; Yang and Cox, 2010). Comparison of the ensuing predictions with experimental measurements will appear in future articles.

The art of formulating reconstruction algorithms or generators for stochastic heterogeneous materials, and related problems in statistical physics, have long histories. One recent piece of relevant work concerns the reconstruction by a variant of the Voronoi polyhedron construction of random granular microstructures in metal alloys from images of serial sections, which were then used in failure simulations (Groeber et al., 2008). Some older work by one of the present authors also used the Voronoi construction to generate stochastic 2D granular microstructures, which were then used as virtual specimens in both probabilistic and Monte Carlo simulations of fatigue crack growth (Cox and Morris, 1987a, 1987b, 1988; Cox, 1989).

The fact that textiles comprise long, continuous fiber bundles of essentially infinite aspect ratio and with complex but systematic interlacing patterns calls for specialized algorithms in a virtual specimen generator. Thus the algorithm developed here is quite different in nature to that developed for granular materials, such as in (Cox, 1989; Groeber et al., 2008), or by other researchers who have been concerned with statistically isotropic multi-phase materials (e.g., (Jiao et al., 2009) and references therein).

In an early study, the statistics of random variations in the orientations of tows in woven textiles were compiled by analyzing optical images of specimens and the potential of the mis-orientations, which are typically substantial, for degrading performance was pointed out (Pastore, 1993). Similar orientation statistics were deduced elsewhere by analyzing complete tow loci, which were determined by fitting images of significant lengths of continuously visible tows in woven and braided textiles (Cox and Dadkhah, 1995; Dadkhah et al., 1995a, 1995b). In the latter body of work, the complete distribution of alignments was used to predict elastic moduli knockdowns (Cox and Dadkhah, 1995), while extreme values in the distributions were used to predict compressive strength and compressive fatigue life, with encouraging agreement with experiment (Dadkhah et al., 1995a, 1995b). The compressive strength and life predictions echo earlier work on tape laminates, where kink band formation is also the governing mechanism in compressive failure; the relationship between strength and misalignment defects in non-textile composites has an old history (Rosen, 1965; Argon, 1972; Budiansky, 1983; Fleck and Budiansky, 1991; Hillig, 1994; Fleck and Shu, 1995).

Of closer pertinence to the present work, data on tow loci fluctuations in a 3D woven composite were used to set up Monte Carlo simulations of stochastic textile specimens under load (Xu et al., 1995). The experimental alignment distributions were recreated in simulations by randomly offsetting the nodes of elements used to model individual tows. Although the term was not in use in the era, each random textile model that was generated was a "virtual specimen" in the sense of the present paper. The simulations were used to predict how Young's modulus varies with the degree of random tow misalignment, and fluctuations in local tensile and shear stresses, which drive tensile and compressive failure. Only orientation defects that lay in the plane of the section image could be determined experimentally; other deviations were not included in the simulations.

Also related to the present work is a theoretical representation of random textile architectures in which the positional deviations of a single tow were represented as continuous stochastic functions along the tow's length (Yushanov and Bogdanovich, 2000). Random deviations were generated via an expansion of tow coordinates in terms of basis functions, with random coefficients. Predictions of how elasticity varies with random tow misalignment were extended to all components of the elasticity tensor.

The present paper focuses exclusively on the problem of generating virtual specimens of stochastic textile composites, with a new method that makes explicit use of experimental data to achieve a calibrated representation of a particular material. The approach makes no *a priori* assumptions regarding the non-stochastic variations of tow loci or their stochastic deviations. The parameters used to model tow loci are established entirely from the direct observation of tow positions in experimental images. The reliance on rich calibrating data is supported by the advent of high resolution computed tomography (CT) using high intensity X-ray beamlines, which can now determine alignment fluctuations in all directions, for all tows throughout a solid specimen (Desplentere et al., 2005; Bale et al., in press). The acquisition of data by synchrotron-based CT is significantly faster than is possible by traditional methods such as imaging sections (Yurgatis, 1987).

By exploiting rich experimental data, the approach is applicable with equal accuracy and efficiency to tows following, e.g., sinusoidal, triangular, square, or irregular waveforms without any increase in the model's complexity, i.e., the number of parameters needed to generate replicas. This is an important distinction from approaches that utilize assumed spatial forms for tow positions, such as harmonic series, which would require a rapidly increasing number of parameters to track loci with complex variations. Thus the approach is applicable to generic weaves and braids, whose tows might follow arbitrary waveforms.

The virtual specimen generator exploits a Markov Chain formulation to generate fluctuations in the coordinates of any tow axis by marching systematically along the tow's length.[1] The Markov Chain formulation is very efficient and suited physically to the textile reconstruction problem, provided the dominant correlations are those along a tow, with correlations between tows relatively weak. The degree to which this condition is satisfied is established for a particular weave type. Where inter-tow correlations are significant, a simple variant of the Markov chain method is proposed.

The Markov Chain formulation is based on a simple ansatz for the Probability Transition Matrix, whose elements are generated from a small set of parameters in such a way that (1) the equilibrium probability density matrix for the chain variable has the datum root mean square deviation (RMSD) for the stochastic coordinate deviation being regenerated and (2) the characteristic decay length (correlation length) for correlations between the values taken by the stochastic quantity at different points along a tow matches the datum correlation length. The formulation successfully reproduces any target tow statistics.

2. The experimental data set

2.1. Subject material

T300 carbon fiber tows were rigidified by a coating of SiC deposited by chemical vapor infiltration. By imaging a preform that is only partially combined with matrix, with most inter-tow volume left void, very clean definition of tows could be obtained. At the same time, rigidifying preserves the preform in the same geometrical state that it would possess if ceramic matrix formation was continued until all space was occupied.

Tows in the imaged textile possess approximately, but not perfectly, elliptical cross-sections. The tows fit together snugly in the woven pattern by a system of approximately periodic undulations, twisting motions, and variations in cross-sectional area and aspect ratio (Fig. 1a). These tow motions and shapes were summarized in (Bale et al., in press) by fitting ellipses to the tow cross-sections and recording variations of the ellipse centroid, area, orientation, and aspect ratio continuously along each tow's length (e.g., color-coded tow loci in Fig. 1a).

Although the cross-sections were not exactly elliptical, a reconstruction algorithm can be successfully developed from the statistics of the fitted ellipses that ultimately recreates non-elliptical tow shapes similar to those in the real specimen and possessing the same values of key statistical measures. This will be reported elsewhere. In this paper, attention is restricted to generating replicas of the tows represented by the one-dimensional (1D) loci of their centroids. Such 1D representations are suitable input for simulations using the Binary Model of textile composites (Cox et al., 1994; Yang and Cox, 2010).

The architecture of the three layer angle interlock material studied in (Bale et al., in press) is shown in Fig. 1. The first step in data analysis and geometry reconstruction is to identify genuses of nominally identical warp and weft tows. As described in (Bale et al., in press), the subject weave contains a single genus of warp tows and three genuses of weft tows, labeled top weft, center weft, and bottom weft (Fig. 1b). The unit cell of the weave contains four warp tows, each with period λ_x in the warp direction and separated by a nominal interval $\lambda_y/4$ in the weft direction (Fig. 1c). Successive warp tows (tows with increasing y coordinate) are shifted by $-\lambda_x/4$ along the warp direction. Weft tows have a period λ_y in the weft direction. The weft tows in any genus are separated by $\lambda_x/4$ in the warp direction. In the coordinate system of Fig. 1, successive weft tows in any genus (tows with increasing x coordinate) are shifted by $-\lambda_y/4$ in the weft direction.

As described in (Bale et al., in press), a global coordinate system (x, y, z) was determined from the image data that is aligned with the average tow orientations and corrects for any misalignment of the specimen relative to the weave during μCT data acquisition. With all data transformed into the aligned system (x, y, z), the periods λ_x and λ_y of the nominal unit cell of the textile were determined and may be regarded as input data in the present analysis (λ_x=11.5 and λ_y=5.1 mm).

2.2. Systematic variations and stochastic deviations

The coordinates of the centroid of any section of a tow are represented by the vector (ξ, z), with $\xi \equiv y$ for warp tows and $\xi \equiv x$ for weft tows. The virtual specimen generator recognizes that the textile architecture imposes periodicity on the structure on average by decomposing (ξ, z) into a non-stochastic, periodic variation (or systematic variation) to which stochastic deviations are added. Thus, using the example of warp tows, the coordinates of the centroids of the jth warp tow at any point n on a convenient grid are written:

$$(y,z)^{(n,j,w)} = \langle (y,z)^{(n,j,w)} \rangle + (\delta y, \delta z)^{(n,j,w)} \tag{1a}$$

where $\langle .. \rangle$ denotes the average over all available data from CT image analysis, and the superscript w denotes "warp tow" (Bale et al., in press). Analogous definitions are made for top, center, and bottom weft tows, with notation tw, cw, and bw replacing w, respectively.

[1] The authors acknowledge the independent formulation of a virtual specimen generator based on a Markov Chain algorithm for laminates of unidirectional plies, in unpublished work by Dr. Dennis Coon.

Since the systematic variation is periodic, then, in the absence of stochastic deviations, any warp or weft tow can be made to coincide with any other tow of the same genus, and possess the same pattern of cross-overs with other tows, by shifting it by some vector $(r\lambda_x/4, s\lambda_y/4)$, with r and s integers. Thus, as also detailed in Bale et al. (in press), systematic variations of the four genuses of tows can be completely specified by the systematic variations of a single "reference" period for each genus of tow. The choice of reference period is arbitrary; one possible choice for the warp tows in illustrated in Fig. 1b.

"Reference period collation" (the collation of data onto a single reference period) maximizes the information that can be extracted from CT imaging data. The reference period concept is also used in generating virtual specimens. The reference periods used for collating data and generating virtual specimens are most conveniently represented by the same grid of N_ϕ equally spaced points, the first lying at one end of the reference period and the other a distance λ/N_ϕ short of the other, with $\lambda=\lambda_x$ for warp tows and $\lambda=\lambda_y$ for weft tows. Thus the second end of the reference period (point $N_\phi+1$) will be equivalent to the first end (first point on the grid) in the periodic structure of a replicated system of tows.

Given a choice of reference period, one can write (continuing the example of warp tows)

$$\langle (y,z)^{(n,j,w)} \rangle = \boldsymbol{u}_\phi^{(w)} + r\frac{\lambda_x}{4}\hat{\boldsymbol{x}} + s\frac{\lambda_y}{4}\hat{\boldsymbol{y}} \tag{1b}$$

where $\boldsymbol{u}_\varphi^{(w)}$ defines the systematic variation in the coordinates of the tow centroids, specified for each of N_ϕ grid points spanning the reference period, and the integers r and s are those that translate any point (n, j, w) on any warp tow to a corresponding point ϕ in the reference period (examples of this translation are shown in Fig. 1b and c).

2.3. The calibration data set

The data required to calibrate the virtual specimen generator consist of the following:

(i) The nominal architecture of the unit cell of the weave and the unit cell periods, λ_x and λ_y.
(ii) The systematic variations of the tow centroids $\boldsymbol{u}_\varphi^{(w)}$, $\boldsymbol{u}_\varphi^{(tw)}$, $\boldsymbol{u}_\varphi^{(cw)}$, and $\boldsymbol{u}_\varphi^{(bw)}$ for each of the warp, top weft, central weft, and bottom weft tows.
(iii) The root mean square deviations (RMSDs) $\sigma_y^{(w)}$, $\sigma_z^{(w)}$, $\sigma_x^{(tw)}$, $\sigma_z^{(tw)}$, $\sigma_x^{(cw)}$, $\sigma_z^{(cw)}$, $\sigma_x^{(bw)}$, and $\sigma_z^{(bw)}$ of the components of the stochastic part of the centroid coordinates for each of the warp, top weft, central weft, and bottom weft tows.
(iv) The correlation lengths $\zeta_y^{(w)}$, $\zeta_z^{(w)}$, $\zeta_x^{(tw)}$, $\zeta_z^{(tw)}$, $\zeta_x^{(cw)}$, $\zeta_z^{(cw)}$, $\zeta_x^{(bw)}$, and $\zeta_z^{(bw)}$ for the components of the stochastic part of the centroid coordinates for each of the warp, top weft, central weft, and bottom weft tows.

Continuing the example of warp tows, the RMSD, $\sigma_\xi^{(w)}$, of a component of the stochastic contribution $(\delta y, \delta z)^{(n,j,w)}$ to the centroid coordinates is defined by

$$\sigma_\xi^{(w)} = \sqrt{\sum (\delta\xi^{(n,j,w)})^2/n_{expt}} \quad (\xi \equiv y \text{ or } \xi \equiv z) \text{ (warp tows)} \tag{2a}$$

where the sum is performed over all n_{expt} available data points from the CT analysis for all warp tows and use has been made of the fact that the mean of $\delta\xi$ is zero.

The correlation length $\zeta_\xi^{(w)}$ is defined in terms of Pearson's correlation parameter for the values of $\delta\xi$ at pairs of data points separated by k data grid points on the same tow

$$C_\xi^{(w)}(k) = \frac{\sum \delta\xi^{(n,j,w)}\delta\xi^{(n+k,j,w)}/nn_{expt}}{(\sigma_\xi^{(w)})^2} \tag{2b}$$

where the sum is performed over all nn_{expt} available pairs of data points $\{(n, j), (n, j+k)\}$ on all warp tows (Bale et al., in press). As k increases, $C_\xi^{(w)}$ generally decreases, indicating that the coordinate deviations on a tow become uncorrelated for well separated points. For small k, the decrease is approximately linear:

$$C_\xi^{(w)}(k) \approx 1 - k\delta/\zeta_\xi^{(w)} \tag{2c}$$

where δ is the distance between successive data grid points and $\zeta_\xi^{(w)}$, a constant, is the correlation length for fluctuations of the ith coordinate of the centroid of warp tows. The correlation length conveys a physical property of the tow coordinate deviations and is independent of the choice of grid spacing, δ, that was used in analyzing the statistics of experimental data. The correlation length is distinct from the wavelength of systematic coordinate variations; unlike the systematic variations, the coordinate deviations need not be periodic or exhibit correlation lengths that are commensurate with the textile unit cell.

The RMSD and correlation parameter have been defined above for warp tows. Similar statistics are defined for the three weft genuses using Eqs. (2a) and (2b) with the notation *tw*, *cw*, or *bw* replacing *w* for top weft, center weft, and bottom weft, respectively.

Additional statistics that can be used in the virtual specimen generator consist of correlations between components of the deviation vectors, $(\delta y, \delta z)^{(n,j,w)}$, $(\delta x, \delta z)^{(n,j,tw)}$, $(\delta x, \delta z)^{(n,j,cw)}$, and $(\delta x, \delta z)^{(n,j,bw)}$ associated with different tow genuses. Of particular interest are the correlations between the stochastic part of the coordinates of a pair of warp and weft tows at the

location of their mutual cross-over. The cross-over points are defined as the intersections of the loci of the centroids of the two tows when projected on the (x, y) plane (cf. Fig. 1c). The correlations at cross-overs were calculated in Bale et al. (in press) for each combination of components of the deviation vectors, using data for all cross-overs formed by all warp tows and all weft tows of one genus. The correlations are

$$C^{(w,weft)}_{\xi,\overline{\xi}} = \frac{\sum \delta\xi^{(w)}\delta\overline{\xi}^{(weft)}/n_{cr}}{\sigma^{(w)}_{\xi}\sigma^{(weft)}_{\overline{\xi}}} \tag{3}$$

where "weft"="tw", "cw", or "bw"; $\delta\xi^{(w)}$ and $\delta\overline{\xi}^{(weft)}$ denote components of the deviations of the warp and weft tows, respectively, at crossovers ($\xi \equiv y$ or z and $\overline{\xi} \equiv x$ or z); and the sum is performed over all n_{cr} crossovers between warp tows and weft tows of the pertinent genus.

2.4. Data for a carbon fiber preform rigidized by SiC

The data used here to illustrate the virtual specimen generator are taken directly from Bale et al. (in press). The wavelengths of the periodic structure of the weave were determined to be $\lambda_x = 11.5$ and $\lambda_y = 5.1$ mm. The average spacing of weft tows in the z-direction is 0.27 mm, but this value is implicit in the calibration data $\boldsymbol{u}^{(tw)}_{\varphi}$, $\boldsymbol{u}^{(cw)}_{\varphi}$, and $\boldsymbol{u}^{(bw)}_{\varphi}$ and need not be supplied separately to the generator.

The systematic (non-stochastic, periodic) variations in the coordinates of tow centroids were recorded at $N_{\phi} = 24$ grid points along the reference period for all tow genuses. These variations are shown for warp tows in Fig. 2. The systematic variations for all four tow genuses are referred to a common origin, so that the relative positioning of different tow genuses through the thickness and in the in-plane directions are correctly stated.

The systematic variations of the coordinates of the centroids of warp tows show approximately sinusoidal variations (Fig. 2). However, sinusoidal fits to the data were not made and are unnecessary and undesirable; the virtual specimen generator uses the spatial variations as they emerge from statistical analysis of image data, without imposing any parametric form. The motion of warp tows in the z-direction exhibits a single cycle per period of the textile architecture (Fig. 2a). Interestingly, its motion in the y-direction exhibits two cycles in the same distance (Fig. 2b).

The systematic variations of the coordinates of the centroids of weft tows show qualitatively similar periodic variations.

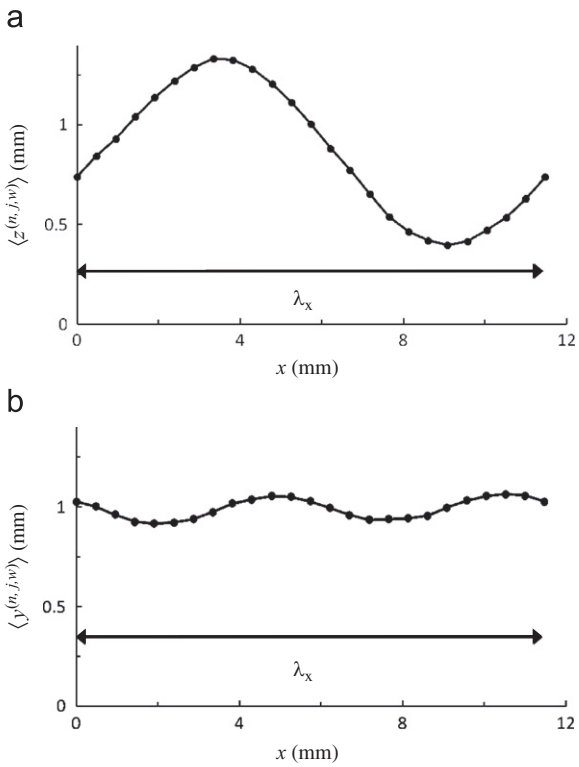

Fig. 2. Experimentally determined non-stochastic, periodic variations of the coordinates of the centroid of warp tows: (a) component in through-thickness direction and (b) component in weft direction.

Table 1
Experimental data: RMSD and correlation length for the stochastic tow parameters.

(a) Warp tows			
$\sigma_y^{(w)}$ (mm)	$\zeta_y^{(w)}$ (mm)	$\sigma_z^{(w)}$ (mm)	$\zeta_z^{(w)}$ (mm)
0.022	3.36	0.035	3.65
(b) Top weft tows			
$\sigma_x^{(tw)}$ (mm)	$\zeta_x^{(tw)}$ (mm)	$\sigma_z^{(tw)}$ (mm)	$\zeta_z^{(tw)}$ (mm)
0.066	3.43	0.029	5.12
(c) Center weft tows			
$\sigma_x^{(cw)}$ (mm)	$\zeta_x^{(cw)}$ (mm)	$\sigma_z^{(cw)}$ (mm)	$\zeta_z^{(cw)}$ (mm)
0.072	3.60	0.016	6.12
(d) Bottom weft tows			
$\sigma_x^{(bw)}$ (mm)	$\zeta_x^{(bw)}$ (mm)	$\sigma_z^{(bw)}$ (mm)	$\zeta_z^{(bw)}$ (mm)
0.073	4.25	0.024	4.64

Table 2
Experimental data: correlations $C_{\xi,\bar{\xi}}^{(w,weft)}$ at cross-overs.

	$\delta x^{(tw)}$	$\delta z^{(tw)}$	$\delta x^{(cw)}$	$\delta z^{(cw)}$	$\delta x^{(bw)}$	$\delta z^{(bw)}$
$\delta y^{(w)}$	−0.161	−0.480	−0.127	−0.230	0.263	−0.295
$\delta z^{(w)}$	0.176	0.900	0.443	0.808	−0.061	0.839

Row label defines component ξ for warp tow; column defines weft genus "weft"="tw", "cw", or "bw" and component $\bar{\xi}$ for weft tow.

The RMSD parameters and correlation lengths for the various components of the deviations of the tow centroid coordinates are shown in Tables 1 and 2.[2] The largest absolute deviations are those of weft tows in the x-direction (lateral displacements in the warp direction). Indicating that good control was maintained in the weaving process, deviations are small compared to the width dimensions of the tows (which are approximately 0.30 mm in the z-direction and 1.57 mm in the in-plane direction). Nevertheless, deviations will commonly occur that are of order of magnitude $2 \times$ RMSD, or approximately 10–20% of the tow width. Such deviations may perturb the local tow density and orientations sufficiently to affect local failure events.

The correlation lengths quoted in the tables are those found by fitting all data from all tows of one genus after collating them into a single set. When data for individual tows are analyzed separately, substantial variation is seen in the deduced correlation lengths. The relation of this variability to the small sample size available from μCT imaging is discussed more fully in Appendix A. A reasonable estimate of the resulting uncertainty in the deduced correlation lengths is $\pm 25\%$. This uncertainty remains small compared to the difference in the correlation lengths for warp and weft tow genuses.

The correlations $C_{\xi,\bar{\xi}}^{(w,weft)}$ between different components of the deviations at cross-overs are negligible, except between the component in the z-direction for different tows (Table 2). The impact of these correlation values on the formulation of the virtual specimen generator are discussed below.

3. A virtual specimen generator

The virtual specimen generator presented here prepares the tow element set needed for Binary Model simulations of textile composites. In the Binary Model, the tow elements are strings of one-dimensional line elements, which are combined with solid effective medium elements that fill out the external shape of a specimen or component (Cox et al., 1994; Xu et al., 1995; Yang and Cox, 2010). The tow elements are formed by interpolating, if necessary, among the coordinates generated for the centroids or axes of warp and weft tows by the virtual specimen generator. The virtual specimen generator uses a random number generator to create specific instances of random tow geometries, whose statistics are the same as those prescribed by the calibrating data.

[2] The numbers presented in Tables 1 and 2 are slightly different to those reported in Bale et al., due to a minor error in data analysis, which is now corrected. The changes in most numbers are small. Changes in some correlation lengths are larger, which reflects the sensitivity of the deduced correlation lengths to the values of the input data, as discussed in Appendix A.

To distinguish variables that describe the product of the generator from similar variables that describe the original data, the former are denoted by symbols that include a tilde. It is also convenient (although not necessary) to base the virtual specimen generator on a grid with the same spacing, δ, as that used for analyzing image data. Thus, for example, the regenerated deviation vector at the nth grid point along the jth warp tow is denoted $(\tilde{y},\tilde{z})^{(n,j,w)}$. But note that the total number and lengths of tows referred to by the superscript (n, j, w) will generally be different from those in the original data set: the virtual specimen generator can generate specimens of any size.

In generating tow axes, it is assumed that

(a1) the distribution of any component of the recreated deviations, $\delta\tilde{\xi}$ (e.g., $\tilde{\xi}\equiv y$ or z for warp tows), is the same for all data points on tows of the same genus;
(a2) the different components $\delta\tilde{\xi}$at each grid point are statistically independent of one another;
(a3) the values taken by each component $\delta\tilde{\xi}$ at different points on the same tow are correlated to a degree that diminishes with the separation of the points;
(a4) each component $\delta\tilde{\xi}$ takes statistically independent values on different tows, whether the tows are of the same or different genus.

Assumption (a3) reflects the fact that nearby points along the same tow are likely to deviate from the average tow locus in a similar way, because they are connected by the fibers in the tow. For example, if the axis of a tow is displaced randomly at some point, the entire tow is likely to be pulled in the same direction over a significant neighboring interval, due to the continuity of the fibers.

With assumptions (a1)–(a3) in place, two cases are considered below, the first taking assumption (a4) as stated above and the second introducing an additional modifying assumption:

(a4′) The through-thickness components $\delta\tilde{z}$ of the deviations of a warp tow and a weft tow are correlated as prescribed by the calibration parameter $C_{z,z}^{(w,\mathrm{weft})}$ of Eq. (3).

The last assumption (a4′) introduces a significant complication.

3.1. Systematic coordinate variations

For warp tows, Eq. (1b) serves as the first part of the generation process. It creates the periodic, non-stochastic (systematic) contribution, $\langle(\tilde{y},\tilde{z})^{(n,j,w)}\rangle$ to the tow coordinates at any point (n, j) on the jth warp tow by translating the coordinates $\boldsymbol{u}_{\varphi}^{(w)}$ of the reference point (n_{ϕ}, w_{ϕ}) through whatever lattice vector is required to reach (n, j) (e.g., Fig. 1c). Analogous procedures generate systematic coordinates for other tow genuses.

3.2. Stochastic deviations of tow centroids—uncorrelated tows

The virtual specimen generator uses a Monte Carlo method to prescribe the stochastic parts of the coordinates of tow centroids, moving sequentially along each tow in turn. For the jth warp tow, for example, the generator prescribes $(\delta\tilde{y},\delta\tilde{z})^{(n,j,w)}$ at grid points $(1, j)$, $(2, j)$, … etc., beginning at one end of the tow and proceeding to the other. Consistently with assumptions (a1)–(a4), the sequence, $(\delta\tilde{y},\delta\tilde{z})^{(1,j,w)}$, $(\delta\tilde{y},\delta\tilde{z})^{(2,j,w)}$, … , of generated random numbers is assumed to constitute a "stationary Markov process" (whose meaning is elaborated below). Computation proceeds by discretizing $\delta\tilde{\xi}^{(n,j,w)}$ ($\xi\equiv y$ or z for warp tows) onto the values $\{-ma,\ -(m-1)a,\ ..\ ,\ 0,\ ..\ ,(m-1)a,\ ma\}$, with $ma=3\sigma_{\xi}^{(w)}$. This choice allows fluctuations over three experimentally determined standard deviations. That deviations cannot exceed 3σ is consistent with experimental data: plots of the distribution of measured deviations confirm that distributions are normal, except that they are truncated at between 2σ and 3σ (Fig. 10 of Bale et al. (in press)). The constraint of the textile fabric apparently prevents larger deviations.

The Markov chain paradigm is similar for all tow genuses. Therefore, a simplified notation is used for new symbols introduced in the following, which omits explicit reference to tow number, j, and genus (e.g., "w" for warp).

The distribution of $\delta\tilde{\xi}^{(n,j,w)}$ is represented by the column vector:

$$P_i^{(n)}=\left|\ p_m^{(n)}\quad p_{m\text{-}1}^{(n)}\quad\cdots\quad p_0^{(n)}\quad\cdots\quad p_{-m+1}^{(n)}\quad p_{-m}^{(n)}\ \right|^T \tag{4a}$$

where superscript T denotes the transpose. The Markov process is represented by the operation

$$P_i^{(n+1)}=AP_i^{(n)} \tag{4b}$$

with A the probability transition matrix

$$A=\begin{vmatrix} A_{m,m} & A_{m,m-1} & . & . & . & . & A_{m,-m} \\ . & A_{m-1,m-1} & . & . & . & . & . \\ . & . & . & . & . & . & . \\ . & . & . & A_{0,0} & . & . & . \\ . & . & . & . & . & . & . \\ . & . & . & . & A_{-m+1,-m+1} & A_{-m+1,-m} & \\ A_{-m,m} & . & . & . & . & A_{-m,-m} & \end{vmatrix}. \tag{4c}$$

The process is Markovian in that $P_i^{(n+1)}$ is assumed to depend only on $P_i^{(n)}$ and not on the distribution of $\delta\tilde{\xi}^{(n,j,w)}$ at any prior point; and, since A is assumed to be independent of n for tows in a given genus, the Markov process is also stationary.

The element $A_{k,k'}$ of A defines the conditional probability:

$$\Pr\{\delta\tilde{\xi}^{(n+1,j,w)}=ka \,|\, \delta\tilde{\xi}^{(n,j,w)}=k'a\} \tag{5}$$

i.e., the probability that $\delta\tilde{\xi}^{(n,j,w)}$ will take the value ka at the $(n+1)$th grid point, given that it had the value $k'a$ at the nth grid point. Therefore, $0\le A_{k,k'}\le 1$ and all columns of A sum to unity.

3.2.1. Canonical forms for the probability transition matrix

A probability transition matrix is sought that reproduces two statistics of experimental data, namely the RMSD, $\sigma_\xi^{(w)}$, and the correlation length, $\zeta_\xi^{(w)}$ ($\xi\equiv y$ or z) (returning to the example of warp tows). The required fit to $\sigma_\xi^{(w)}$ and $\zeta_\xi^{(w)}$ is achieved by controlling the asymptotic behavior of the probability distribution produced by the stationary Markov operator A.

When A acts iteratively a large number of times (repeated application of Eq. (4b)), the resulting distribution vector approaches asymptotically the eigenvector of A that is associated with the largest eigenvalue of A. (Any initial distribution vector can be written as a linear combination of the eigenvectors, q_k, of A, $k=1,\ \dots\ ,2m+1$. When A multiplies the initial vector, the coefficient of the kth eigenvector in the linear combination is multiplied by the corresponding eigenvalue, μ_k. If this is repeated n times, the factor multiplying each coefficient is μ_k^n. For large n, the term for which μ_k is largest dominates.) Let $\mu^>$ denote the largest eigenvalue and $p^>$ the corresponding eigenvector (the asymptotic distribution). Because the elements of A are all positive and columns sum to unity, $\mu^>=1$ (the Perron–Frebonius theorem) (Perron, 1907; Frobenius, 1912). A feature of the virtual specimen generator introduced below is that it is defined always to act in the asymptotic regime; the generated distribution for $\tilde{\xi}_i$ at any data point is always $p^>$ when sampled over many generated replicas.

The RMSD achieved by the Markov Chain can be expressed in terms of the elements of $p^>$:

$$\tilde{\sigma}_\xi^{(w)}=\sqrt{\langle\delta\tilde{\xi}^2\rangle}=\left[a^2\frac{\sum_k k^2\Pr\{\delta\tilde{\xi}^{(n,j,w)}=ka\}}{\sum_k\Pr\{\delta\tilde{\xi}^{(n,j,w)}=ka\}}\right]^{1/2} \tag{6a}$$

where $\langle..\rangle$ denotes expectation value and $\Pr\{\delta\tilde{\xi}^{(n,j,w)}=ka\}$ is the probability of $\delta\tilde{\xi}^{(n,j,w)}$ taking the discrete value ka at grid point (n,j). In the steady-state regime of the Markov process, where $\Pr\{\delta\tilde{\xi}^{(n,j,w)}=ka\}=p_k^>$ (the kth element of $p^>$), one has

$$\tilde{\sigma}_\xi^{(w)}=a\sqrt{\sum_k k^2 p_k^>} \tag{6b}$$

The correlation achieved between values of $\delta\tilde{\xi}^{(n,j,w)}$ at successive data points is

$$\tilde{C}_\xi^{(n,n+1,j,w)}=\langle\delta\tilde{\xi}^{(n,j,w)}\delta\tilde{\xi}^{(n+1,j,w)}\rangle/(\tilde{\sigma}_\xi^{(w)})^2=\left(\frac{a}{\tilde{\sigma}_\xi^{(w)}}\right)^2\frac{\sum_{k,k'}kk'\Pr\{(\delta\tilde{\xi}^{(n,j,w)}=ka)\&(\delta\tilde{\xi}^{(n+1,j,w)}=k'a)\}}{\sum_{k,k'}\Pr\{(\delta\tilde{\xi}^{(n,j,w)}=ka)\&(\delta\tilde{\xi}^{(n+1,j,w)}=k'a)\}} \tag{7a}$$

where $\Pr\{(\delta\tilde{\xi}^{(n,j,w)}=ka)\ \&\ (\delta\tilde{\xi}^{(n+1,j,w)}=k'a)\}$ is the joint probability of $\delta\tilde{\xi}^{(n,j,w)}$ taking the discrete values ka and $k'a$ at successive grid points along the tow. In the steady-state regime

$$\Pr\{(\delta\tilde{\xi}^{(n,j,w)}=ka)\&(\delta\tilde{\xi}^{(n+1,j,w)}=k'a)\}=\Pr\{\delta\tilde{\xi}^{(n+1,j,w)}=k'a\,|\,\delta\tilde{\xi}^{(n,j,w)}=ka\}\Pr\{\delta\tilde{\xi}^{(n,j,w)}=ka\}=A_{k',k}p_k^> \tag{7b}$$

and thus

$$\sum_{k,k'}\Pr\{(\delta\tilde{\xi}^{(n,j,w)}=ka)\&(\delta\tilde{\xi}^{(n+1,j,w)}=k'a)\}=\mu^>\sum_k p_k^>=1 \tag{7c}$$

where the last equality follows from the fact that $p^{>}$ represents a set of normalized probabilities. Thence

$$\tilde{C}_{\xi}^{(n,n+1,j,w)} = \frac{\langle \delta\tilde{\xi}^{(n,j,w)} \delta\tilde{\xi}^{(n+1,j,w)} \rangle}{(\tilde{\sigma}_{\xi}^{(w)})^2} = \left(\frac{a}{\tilde{\sigma}_{\xi}^{(w)}}\right)^2 \sum_{k,k'} k k' p_k^{>} A_{k',k} \tag{7d}$$

which, following from the assumptions of the formulation, is independent of grid number, n, or tow number, j.

Consider now the $(2m+1)\times(2m+1)$ tridiagonal probability transition matrix

$$A_0 = \begin{vmatrix} \alpha & \gamma & 0 & . & & & & & . & 0 \\ \beta' & \alpha & \gamma & 0 & . & & & & & . \\ 0 & \beta & \alpha & . & . & . & & & & \\ . & 0 & . & . & \gamma & 0 & . & & & \\ & . & . & \beta & \alpha & \delta & 0 & . & & \\ & & . & 0 & \beta & \alpha & \beta & 0 & . & \\ & & & . & 0 & \delta & \alpha & \beta & . & . \\ & & & & . & 0 & \gamma & . & . & 0 & . \\ & & & & & . & . & . & \alpha & \beta & 0 \\ . & & & & & & & 0 & \gamma & \alpha & \beta' \\ 0 & . & & & & & & . & 0 & \gamma & \alpha \end{vmatrix} \tag{8}$$

where all elements take values in [0, 1] and all columns add to unity. The inversion symmetry of A_0 ($A_{k,k'}=A_{-k,-k'}$, $0\le k\le m$, $0\le k'\le m$) assures that, if A_0 is applied as a generator, $\delta\tilde{\xi}^{(n,j,w)}$ will be distributed evenly about zero.

The generated deviation, $\tilde{\sigma}_{\xi}$ (omitting notation referring to tow type), is controlled by varying the relative magnitudes of β and γ, with $\beta>\gamma$ for distributions that are peaked at zero. As $\beta-\gamma$ increases from zero at fixed α, $\tilde{\sigma}_{\xi}$ decreases, because $\beta>\gamma$ favors a return towards $\delta\tilde{\xi}=0$ at each step in the Markov sequence. In the limit $\beta=\gamma$, each value of $\delta\tilde{\xi}$ in the discrete set $\{-ma, .. , ma\}$ is approximately equally favored and $\tilde{\sigma}_i$ takes a value given approximately by

$$\sigma_{max} = \sqrt{\frac{\sum_{k=-m}^{m} (ma)^2}{2m+1}} = \sqrt{\frac{m(m+1)}{3}}a \tag{9}$$

(The dominant eigenvector of A_0 only has equal elements when $\beta=\gamma$ in the limit $m\to\infty$; the discrepancy between Eq. (9) and the limiting value of $\tilde{\sigma}_i$ is caused by end effects, i.e., the necessity of modifying the transition probabilities for the extreme states in $P_i^{(n)}$ to maintain normalization.)

Fig. 3a shows the variation in $\tilde{\sigma}_{\xi}/\sigma_{max}$ as β is varied over its full range subject to $\beta\ge\gamma$, with α fixed at 0.9 and $m=10$. If α is varied, $\tilde{\sigma}_{\xi}/\sigma_{max}$ remains unchanged provided β is also changed to conserve the ratio $\beta/(1-\alpha)$. Variations of $\tilde{\sigma}_{\xi}/\sigma_{max}$ with m are insignificant. With an appropriate choice of m and a, a value of β can be found to achieve any target RMSD.

Whatever the values of α and $\beta-\gamma$, the correlation parameter $\tilde{C}_{\xi}^{(n,n+1)}$ (again omitting reference to tow type) remains numerically close to unity. If $\alpha\to1$, $\tilde{C}_{\xi}^{(n,n+1)}\to1$; successive values of $\delta\tilde{\xi}$ in the Markov sequence are perfectly correlated. The value of $\tilde{C}_{\xi}^{(n,n+1)}$ can be reduced slightly by decreasing α, but, for the tridiagonal form chosen in Eq. (8), the reduction is limited by the fact that successive values of $\delta\tilde{\xi}$ can never be separated by more than a. Thus the tridiagonal form of A_0 can generate distributions with any RMSD, but does not give independent control of the correlation parameter.

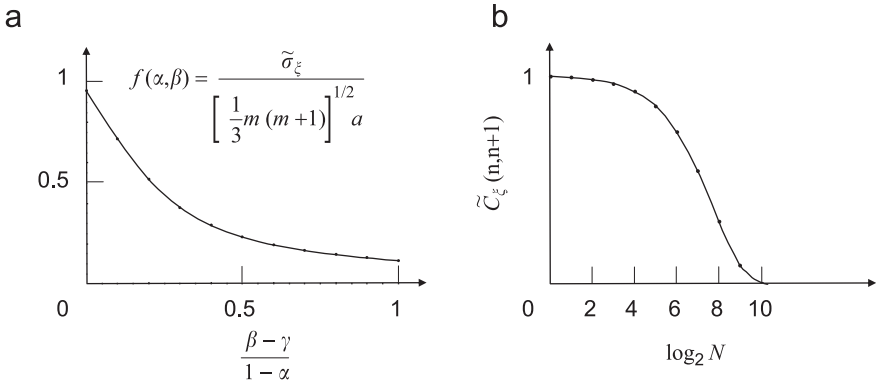

Fig. 3. (a) Root mean square deviation of steady-state distribution generated by the tridiagonal probability transition matrix A_0 vs. $(\beta-\gamma)/(1-\alpha)$. (b) The correlation parameter generated by the probability transition matrix A_N vs. the power N. Both cases for the choice $\alpha=0.9$, $m=10$.

Consider therefore the probability transition matrix

$$A_N = A_0^N \tag{10}$$

which represents N iterative applications of the tridiagonal transition matrix A_0. First note that

$$A_N p^{>} = A_0 p^{>} \tag{11}$$

i.e., in the steady state regime, A_N generates the same distribution of $\delta\tilde{\xi}$ as A_0. Therefore, if A_0 is chosen to achieve $\tilde{\sigma}_\xi = \sigma_\xi^{(w)}$, then A_N will also achieve $\tilde{\sigma}_\xi = \sigma_\xi^{(w)}$. The correlation parameter, in contrast, will decrease monotonically as N increases; memory of the initial state in the Markov chain must fade cumulatively with each transition to a new state, $P_i^{(n)} \to A_0 P_i^{(n)}$. Even if α is very close to unity, $\tilde{C}_\xi^{(n,n+1)}$ can be reduced to zero if N is chosen sufficiently large (Fig. 3b).

3.2.2. Calibrating the Markov chain

First establish a satisfactory mesh for the discrete variable $\delta\xi$ by requiring a and m to satisfy

$$\sigma_\xi = \frac{ma}{3} \tag{12}$$

(suppressing the reference to tow type) so that the discrete space can represent values of $\delta\xi$ up to 3 deviations removed from the mean. Subject to Eq. (12), m and a can be chosen arbitrarily; the choice $m=10$ assures that the spacing between the discrete values allowed for $\delta\tilde{\xi}$ is reasonably small compared to the range of most likely values. The value of a then follows from Eq. (12).

With m and a satisfying Eq. (12), and if $\alpha=0.9$ by choice, the condition

$$\tilde{\sigma}_\xi = \sigma_\xi \tag{13a}$$

reduces to

$$f = \frac{m/3}{\sqrt{\frac{1}{3}m(1+m)}} \approx 0.55 \quad (\text{for } m = 10) \tag{13b}$$

where $f(\beta,\alpha)$ is the function plotted in Fig. 3a. This, together with $\beta+\gamma=1-\alpha$ determines the value of β.

With β set, the power N is determined by requiring that the generated correlation $\tilde{C}_\xi^{(n,n+1)}$, which is plotted in Fig. 3b, equals the experimentally determined statistic C_ξ.

The calibration is repeated for each tow genus, using, for example, the data of Section 2.4.

3.2.3. Operating the virtual specimen generator

The systematic contributions to coordinates are generated by application of Eq. (1b).

The stochastic contributions are generated for each tow by the Monte Carlo method. The statistics of the stochastic coordinates produced by the generator should be uniform for all data points along any tow; there should be no transient period at the beginning of the tow during which the result of the Markov process moves asymptotically towards the steady state distribution $p^{>}$. This is assured by selecting the stochastic coordinate value for the first point on the tow from the distribution $p^{>}$. The set of coordinate values generated for subsequent points on the tow by applying the probability transition matrix will have the same distribution when sampled over many replicas.

Implementation of the Monte Carlo method will refer to the following piecewise constant function derived from a probability density vector, $P=\{p_m, \ldots\ p_{-m}\}^T$:

$$\chi(P;\delta\xi) = \begin{cases} 0 & \delta\xi < -ma \\ \sum_{k'=-m}^{k} p_{k'} & -ma \le \delta\xi < ma \quad \text{where } ka \le \delta\xi < (k+1)a \\ 1 & \delta\xi \ge ma \end{cases} \tag{14}$$

For large m (very fine grid for ξ), this function coincides with the cumulative probability distribution (cpd) for the variable $\delta\xi$ described by P.

The steps taken to fill out the coordinates along a tow are as follows:

1. Generate a uniformly distributed random number, η, using a pseudo-random number generator.
2. By comparing η with the function $\chi(p_{>};\delta\xi)$ generate a coordinate value

$$\delta\tilde{\xi}(1,w) = ka \quad \text{where } \chi(p_{>};ka) \le \eta < \chi(p_{>};(k+1)a) \tag{15a}$$

for the first point $(1, w)$ on a tow from the discrete set $\{-ma, -(m-1)a, .., 0, .., (m-1)a, ma\}$. Denote this value $k_1 a$.
3. Fill out values of $\delta\tilde{\xi}$ for the remaining points on the tow by the following iteration.

Given the value $k_n a$ of $\delta\tilde{\xi}$ at the nth grid point, define the density vector

$$\pi_i^{(n)} = |\,0 \quad \ldots \quad 0 \quad 1 \quad 0 \quad \ldots \quad \ldots \quad 0\,|^T \tag{15b}$$

where the non-zero entry appears at element k_n.

4. Form the density vector

$$P_i^{(n+1)} = A\pi_i^{(n)}. \tag{15c}$$

Choose another random number, η, and determine $\delta\tilde{\xi}(n+1, w)$ by comparing η with $\chi(P_i^{(n+1)}; \delta\xi)$, analogously to Eq. (15a). Denote this value $k_{n+1}a$. Form a vector $\pi_i^{(n+1)}$ with a single non-zero element at k_{n+1} analogously to Eq. (15b).

5. Iterate step 4 until all points on the tow have been filled.

Because the vector $\pi_i^{(n)}$ has only one non-zero entry, Eq. (15c) is a trivial substitution, rather than a matrix multiplication, and the computational effort expended in implementing Eq. (14) and (15) is very slight.

3.3. Eliminating mesh effects

The Markov Chain algorithm successfully reproduces stochastic coordinate deviations that vary along the tow axis in a manner consistent with the target RMSD and correlation length. A typical instance of a stochastic deviation (δx for a central weft tow) is shown in Fig. 4. The large-amplitude, long-wavelength variations visible in Fig. 4 occur over distances along the tow that are comparable to the target correlation length, $\zeta_x^{(cw)}$. However, the algorithm also generates small-amplitude, short-wavelength oscillations, which appear as sharp random spikes on the raw generated curve (the fine line in Fig. 4). The amplitude of the spikes can be reduced by refining the grid for the random variable (increasing m in Eq. (4) while maintaining the condition $ma=3\sigma_x$), and their wavelength depends on the grid density along the tow, λ_y/N_ϕ. Thus the spikes are mesh-dependent.

The spikes are not realistic: a mechanically continuous tow cannot exhibit such sharp variations in its position. The spikes enter through the assumption that the deviations can be regarded as a Markovian process. In the example of Fig. 4, the value δx_k at grid point k depends only on the value δx_{k-1} at grid point $k-1$ and not on the values δx_{k-2} at grid points $k-2$, etc. The Markov Chain generator carries no constraint mimicking the tendency of continuous fibers to remain smooth, which would involve derivatives of the deviations; or, equivalently, the differences $\delta x_{k-1}-\delta x_{k-2}$, i.e., the deviations at earlier grid points in the generation sequence. The generator only carries instructions that generate the longer range variations described by the correlation length, $\zeta_x^{(cw)}$.

The spikes can be smoothed away by applying a local averaging to the generated sequence of deviations. To minimize its effect on the RMSD of the generated deviations, the averaging is made over the squares of the deviations, using a newly formulated algorithm (Appendix B). To avoid affecting the correlations along a tow, the averaging is conducted over gage lengths that are smaller than the datum correlation length of the deviations. The results of a recursive smoothing operation (Appendix B) that uses

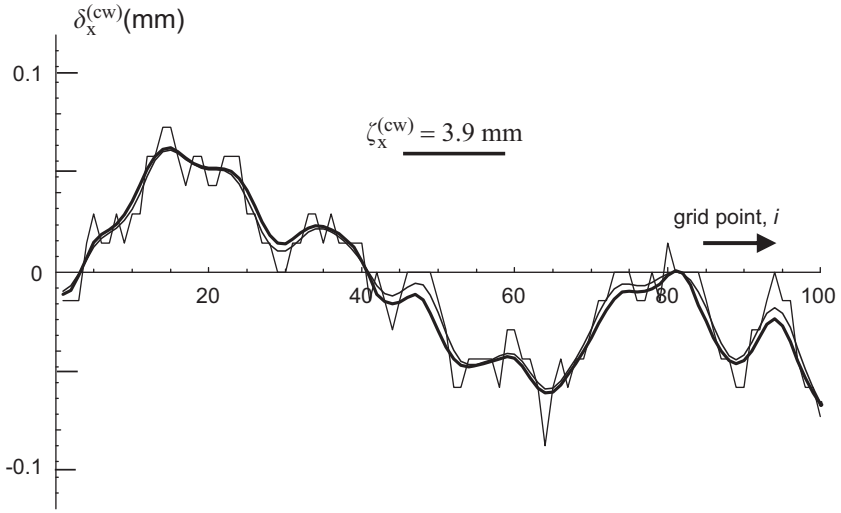

Fig. 4. Smoothing grid effects in generated coordinate deviations: spiked curve is the raw output of the Markov Chain generator; fine smoothed curve is the result of applying a conventional moving average recursively to the deviations; thick smoothed curve is the result of applying the RMSD-conserving average of Appendix B. The recursion depth defined in Appendix B is 4 for each averaging procedure, i.e., a moving average that references grid points $i\pm1$ is applied four times, thus incorporating weighted information from grid points up to $i\pm4$ at any grid point i. The case shown is an example of the deviation in the x coordinate of a central weft tow. The grid index counts grid intervals, which are $\lambda_y/N_\phi=0.21$ mm in length in this example. The bar shows the target correlation length for $\delta x^{(cw)}$.

weighted information across ± 4 grid intervals are shown by the thick curve in Fig. 4: the physically significant large-amplitude, long-wavelength variations remain intact, while the non-physical spikes are reduced to ripples of very small amplitude (a few μm), which will have negligible influence on the predicted mechanical performance of the composite.

3.4. Correlated tows

The geometry generation described above is relatively simple because the deviations in the coordinates of the centroids of different tows are assumed not to be correlated. A single tow can be described by a sequence of variables that progress along its one-dimensional axis, a process that maps conveniently onto the formalism of Markov chains.

When significant correlations do exist between the deviations of different tows, the problem becomes much more complex. In the most general cases, the Markov chain method may no longer be useful. However, under certain circumstances, a minor modification of the procedure described in Section 3.2 proves adequate.

For the ceramic material analyzed by Bale et al. (in press), the only significant correlations between tows of different genus arise between the through-thickness component of the deviations of the centroids, $\delta\tilde{z}$ (Table 2). Consider now the parameter

$$Z = \zeta_z / l_c \tag{16}$$

where ζ_z is the correlation length for the coordinate component δz of a tow and l_c is the spacing between successive cross-overs along the tow. For weft tows in the subject material, $l_c = \lambda_y/4 = 1.3$ mm while the correlation lengths $\zeta_z^{(tw)}$, $\zeta_z^{(cw)}$, and $\zeta_z^{(bw)}$ range from 4.6–6.1 mm, so that the ratio $Z = \zeta_z^{(weft)}/l_c$ is much larger than unity. For warp tows, in contrast, $l_c = \lambda_x/4 = 2.9$ mm while $\zeta_z^{(w)} = 3.7$ mm, and thus $Z = \zeta_z^{(warp)}/l_c \approx 1$. This difference in value of Z implies an hierarchy of influence among tows in which the weft tows are dominant; weft tow deviations are not strongly affected by warp deviations, whereas warp deviations are strongly affected by weft deviations. For such cases, where one tow genus dominates deviations, the following procedure is proposed. Each weft tow is treated as being independent of all other tows and its deviations are generated following the procedure of Section 3.2 (adapted notationally to weft tows). With the weft tow centroid coordinates thus completely stated, the coordinates for warp tows are prescribed as follows.

The non-stochastic, periodic warp tow coordinates are specified as before (Section 3.1); issues arising from correlations affect only deviations, not systematic variations. The warp deviations in the y-direction are also generated as before (Section 3.2); this component of the deviation is statistically independent of the weft tow deviations.

The deviations of the z-coordinate for warp tows are specified first at the locations of cross-overs with weft tows. The warp and weft deviations at any cross-over are assumed to belong to a bivariate density function that possesses the calibrated RMSDs, $\sigma_z^{(w)}$ and $\sigma_z^{(weft)}$ for warp and weft deviations, and the calibrated correlation $C_{z,z}^{(w,\mathrm{weft})}$ between the warp and weft deviations, with "weft" = "tw", "cw", or "bw". If the density function is binormal, then the probability of the warp deviation taking the value $\delta\tilde{z}^{(w)}$ given that the weft deviation has taken the value $\delta\tilde{z}^{(weft)}$ is[3]

$$\Pr\{\delta\tilde{z}^{(w)} \,|\, \delta\tilde{z}^{(weft)}\} = \frac{1}{A}\exp\left[\frac{(\delta\tilde{z}^{(w)} - \mu_w)^2}{\sigma_w^2}\right] \tag{17a}$$

where

$$\mu_w = C_{z,z}^{(w,weft)} \frac{\sigma_z^{(w)}}{\sigma_z^{(weft)}} \delta\tilde{z}^{(weft)} \tag{17b}$$

$$\sigma_w^2 = (1 - (C_{z,z}^{(w,weft)})^2)(\sigma_z^{(w)})^2 \tag{17c}$$

where use has been made of the fact that $\langle \delta\tilde{z}^{(w)} \rangle = \langle \delta\tilde{z}^{(weft)} \rangle = 0$ to simplify these expressions.

Thus, given the generated weft deviation, $\delta\tilde{z}^{(weft)}$, at any cross-over, the warp deviation, $\delta\tilde{z}^{(w)}$, can be determined by generating a random number, μ, and following steps analogous to Eqs. (14) and (15).

Given the warp deviations, $\delta\tilde{z}^{(w)}(1)$ and $\delta\tilde{z}^{(w)}(2)$, at two consecutive cross-overs located at x_1 and x_2 along a warp tow, the warp deviation at any grid point, n, lying between these two cross-overs is determined by interpolation between the two cross-over points:

$$\delta\tilde{z}^{(w,n)} = fn(\delta\tilde{z}^{(w)}(2), \delta\tilde{z}^{(w)}(1)) \tag{18}$$

where fn represents an interpolating function. This expedient procedure generates deviations with a correlation length comparable to the separation of cross-overs encountered along the warp tow, which is consistent with the data of Table 1 for the ceramic textile preform studied by Bale et al. (in press). An interpolation function that tends to preserve the target RMSD for the deviations is presented in Appendix B.

[3] e.g., http://www.aiaccess.net/English/Glossaries/GlosMod/e_gm_binormal_distri.htm

3.5. Confirmation of target statistics

To test whether the Markov chain procedure achieves the target statistics, i.e., the statistics supplied from experiment as the input for the generator, a statistical analysis was performed of a large ensemble (1000 members) of generated tow models. Each member of the ensemble consisted of a single unit cell of the textile architecture, cut out of an area equivalent to a 3×3 set of unit cells. Generating a larger specimen than the area analyzed eliminates any minor edge effects, which can arise in the procedure used when warp and weft deviations are treated as correlated.

The systematic coordinate functions were re-computed for the output virtual specimens as the average of the generated stochastic coordinate functions, following the same procedure that was originally used to analyze the μCT data (Fig. 1c). The deviations of tow loci were then computed relative to these output systematic coordinate functions and their statistics collated.

As one would expect, the output systematic coordinate functions were identical to the input systematic coordinate functions: deviations are always symmetrically distributed around zero and therefore their average is zero.

3.5.1. Deviations on uncorrelated tows

For tows that are statistically independent of one another (uncorrelated tows), the Markov Chain algorithm correctly reproduces the statistics of both components of the coordinate deviations, on average. Typical results are illustrated in Figs. 5 and 6, using data for warp tows that were generated as independent entities, without correlation to weft tows.

Histograms of the RMSD over the ensemble of virtual specimens are centered on the target RMSD (the experimental datum), both for deviations that are left unsmoothed and deviations that have been smoothed by the RMSD-conserving formula of Appendix B (Figs. 5a and b and 6a and b). Thus the RMSD-conserving smoothing rule has had no effect on the generated statistics.

The RMSD exhibits a relatively wide distribution over the ensemble of virtual specimens, because each specimen is relatively small. The width of the distribution of the RMSD will decrease approximately as the reciprocal of the square root of the specimen size. The width of the distribution for the case shown reflects the fact that significant specimen-to-specimen variation in a stochastic reinforcement architecture is implied when the specimen gage section is of order of magnitude 30×15 mm^2.

Histograms of correlation lengths for unsmoothed generated deviations are also centered on the experimental target (Figs. 5c and d). When smoothing is applied, the lowest values of correlation length are no longer present, but the

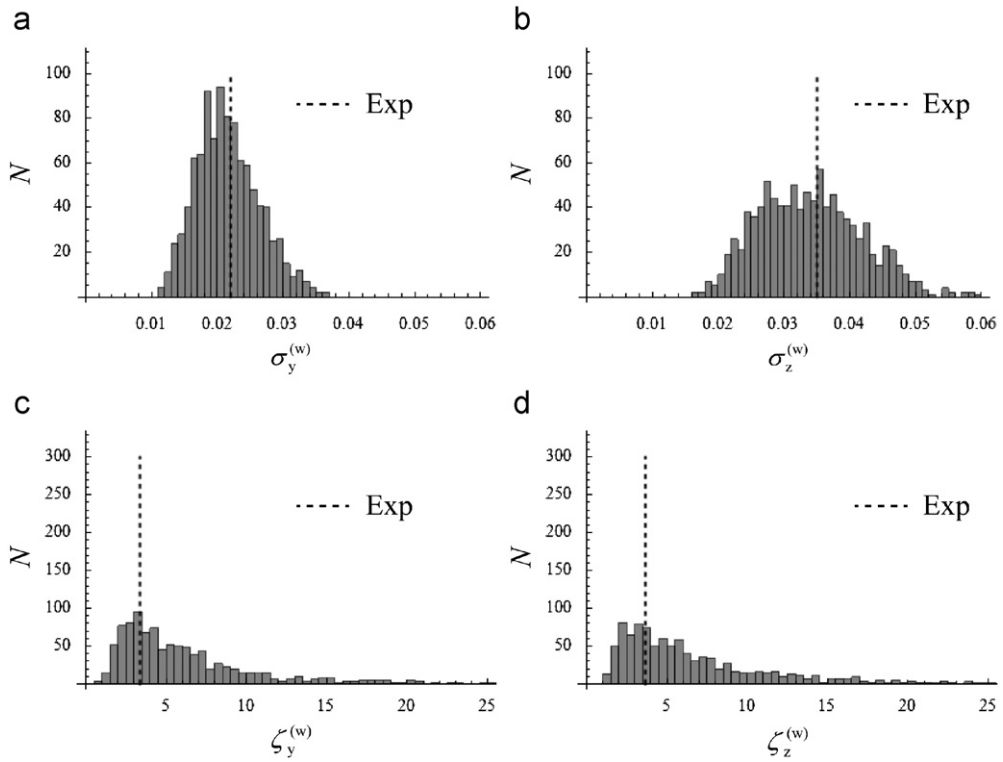

Fig. 5. Histograms of (a) and (b) the RMSD and (c) and (d) the correlation length of the deviations of warp tows in an ensemble of 1000 generated virtual specimens, each of which is one unit cell in size. The vertical dashed lines mark the target (experimental) values. Deviations generated without correlation to weft tow deviations. No smoothing applied.

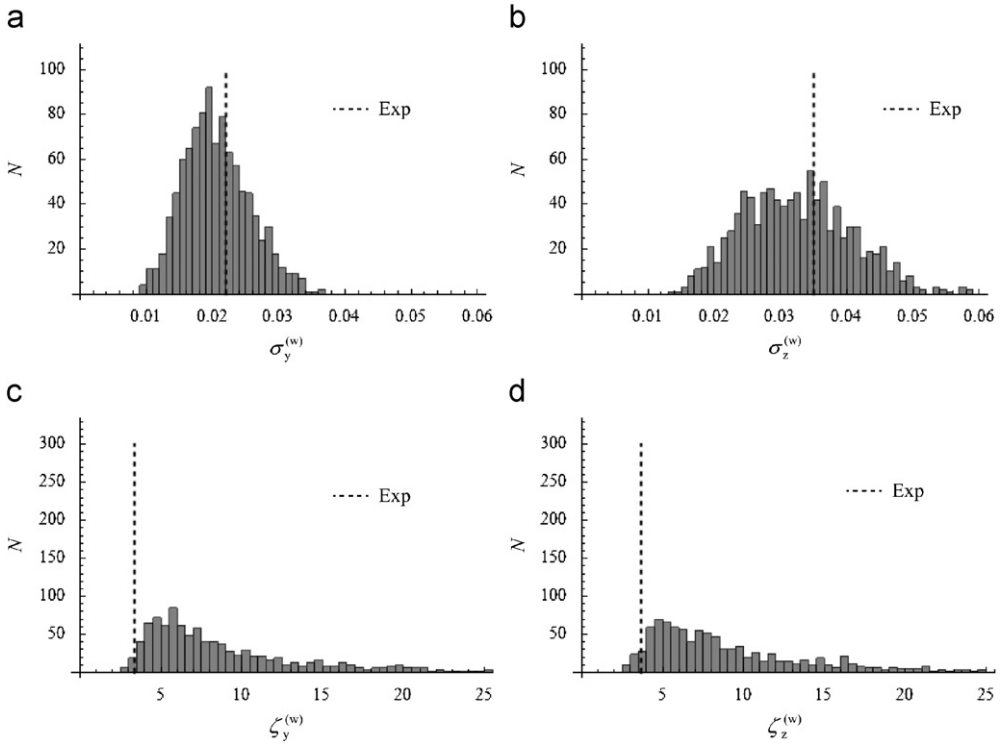

Fig. 6. Histograms of (a) and (b) the RMSD and (c) and (d) the correlation length of the deviations of warp tows in an ensemble of 1000 generated virtual specimens, each of which is one unit cell in size. The vertical dashed lines mark the target (experimental) values. Deviations generated without correlation to weft tow deviations. RMSD-conserving smoothing applied (see Appendix B).

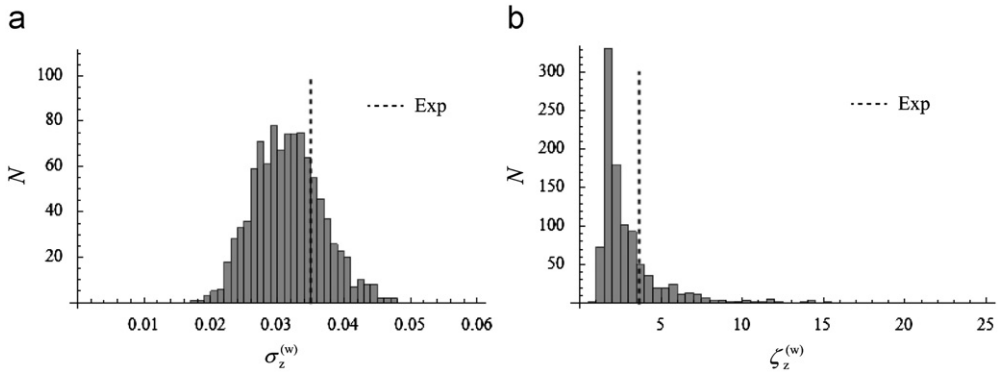

Fig. 7. Histograms of (a) the RMSD and (b) the correlation length of the deviations of warp tows in an ensemble of 1000 generated virtual specimens, each of which is one unit cell in size. The vertical dashed lines mark the target (experimental) values. Deviations generated with correlation to weft tow deviations by the procedure of Section 3.4. No smoothing applied.

generated lengths remain satisfactorily close to the target (Figs. 6c and d). In assessing the quality of reproduction of the target correlation length, account must be taken of the substantial variability found in both experimental and generated correlation lengths. In particular, occasional very high values of the correlation length are expected when the statistics are generated from small specimens (see Appendix A).

3.5.2. *Deviations on correlated tows*

When the z-component of warp tow deviations was computed using the procedure of Section 3.4 for the case of strong correlation between warp and weft tows, the RMSD-conserving interpolation rule (Appendix B) was applied, which is an additional source of possible discrepancy between generated and target statistics (Fig. 7).

The histogram of the RMSD moves to slightly lower values, but remains satisfactorily distributed about the target RMSD. The RMSD-conserving interpolation formula works well. The histogram of correlation lengths becomes somewhat lower than the target correlation length, because the procedure for treating correlation with the weft tows interpolates values between warp-weft crossovers. Therefore, the case that the generated correlation length significantly exceeds the distance of separation of crossovers is relatively improbable.

4. Use of generated stochastic microstructures as virtual specimens

The stochastic 1D tow representations that are generated by the Markov Chain algorithm are suitable for immediate insertion into Binary Model simulations of textile composite behavior. The Binary Model is a low-order representation of a textile, in which the axial properties of tows are introduced through 1D string elements, while the matrix-dominated properties are introduced via 3D effective medium elements (Cox et al., 1994; Xu et al., 1995; Yang and Cox, 2003, 2010).

A few simple additional steps are required to form a virtual specimen from a regenerated tow structure. First, a tow structure is generated that is larger than the specimen in both in-plane directions. Second, this oversized structure is trimmed so that tows that are intersected by any specimen surface end exactly on that surface, with a new node introduced there if necessary (as is usually the case). The trimming operation can introduce features such as internal holes or specimen surfaces that are oriented at any angle to the nominal fiber directions. Third, an effective medium mesh is generated that follows the external shape of the specimen. Finally, a finite element model is formed by assigning constitutive laws to the tow and effective medium elements and combining the two meshes into a single problem by the method of multi-point constraints. An example of a virtual specimen appears in Fig. 8. Details of simulations and comparison with experimental measurements of strain fields and failure will be presented elsewhere.

While the Binary Model cannot predict all details of local stress and strain fields within a composite, it can predict local variations sufficiently well to predict the effects of the textile architecture on many global properties of interest (Xu et al., 1995; Yang and Cox, 2010). Key to predicting local strain variations is the use of gage-averaging to remove mesh effects associated with the 1D tow elements. Gage-averaging also provides a physically rational metric for predicting local failure (Yang and Cox, 2003, 2010). Composite property predictions that can be made using the virtual specimens of this paper include:

(i) the effect of tow variability on the composite elastic moduli (see also Xu et al., 1995) and
(ii) the effect of tow misalignment relative to the nominal tow direction on compressive failure due to kink band formation, in monotonic or cyclic loading (Dadkhah et al., 1995b; Xu et al., 1995).

5. Combination with long-range stochastic deviations

The method presented here has the limitation that it cannot regenerate systematic distortions that occur over spatial scales much larger than the textile unit cell, because information about large-scale distortions cannot be found in image data captured by the small specimens that can be scanned by high-resolution tomography. For the material for which data were used here as an example, supplementary optical images indicate the absence of long-range distortions (Bale et al., in press). If long-range distortions were detected in a different material, a possible strategy for a virtual specimen generator would be to superimpose the measured long-range distortions on the coordinates generated by the generator described in

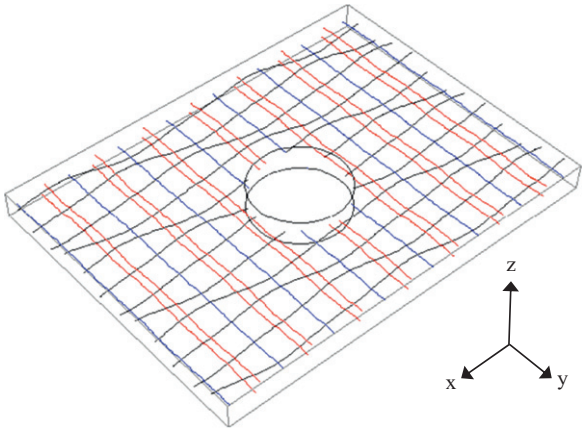

Fig. 8. Typical virtual specimen: stochastic 1D tow representations in a cuboidal specimen with a hole in the center.

this paper, i.e., to assume that the deviations dealt with here, with relatively short-range correlations, are statistically uncorrelated with long-range deviations.

6. Concluding remarks

The strategy proposed here for generating instances of textile reinforcement with stochastic geometry relies entirely on experimental data. One rich source of data is modern high-resolution 3D imaging. Models of the mechanics of fiber tow or preform deformation, which have been the basis for most other attempts to generate realistic geometric models of textiles (mainly non-stochastic models), are not used. Therefore there is no risk of errors flowing from uncertainty in the constitutive laws assumed to characterize such deformation, or in misrepresentation of the conditions during which preform fabrication or handling are carried out, including loading conditions or the presence or absence of lubricating agents. The preform is analyzed as it is, in its final disposition.

The use of reference period collation to divide the coordinates of tow centroids into non-stochastic, periodic (or systematic) variations and stochastic, non-periodic deviations results in a virtual specimen generation algorithm (or reconstruction algorithm) that is as simple as possible, yet can generate specimens much larger than those for which image data were acquired. The data required to calibrate the model consist of the systematic variation of a variable defined over a single reference period (typically 24 data points) plus the RMSD and correlation length for the deviations in the variable (two scalar parameters), repeated for each tow genus, and the two components ξ and z of the coordinates of the centroids ($\xi=y$ for warp tows and $\xi=x$ for weft tows).

If significant correlations exist between deviations on different tows, virtual specimen generation will generally require solution of multi-dimensional problems, rather than being separable into one-dimensional problems that can be treated by the Markov Chain approach. However, for the illustrative C/SiC material of this paper, the only significant correlation between tows could be treated by a simple adaptation of the Markov Chain approach, because of the statistical dominance of one tow over the other.

The loci of tow centroids generated here will supply Binary Model simulations of the textile composite with complete one-dimensional tow meshes. Procedures exactly analogous to those detailed here could also be followed to generate solid tow models; the area, aspect ratio, and orientation of cross-sections of each tow are stochastic variables that can be generated along the tow by Markov operators identical in form to those of Eqs. (8) and (10). The generation of virtual specimens with three-dimensional tow models via this procedure will be described elsewhere.

Acknowledgments

This work was supported by the Air Force Office of Scientific Research (Dr. Ali Sayir) and NASA (Dr. Anthony Calomino) under the National Hypersonics Science Center for Materials and Structures (AFOSR Contract no. FA9550-09-1-0477).

Appendix A. Uncertainty in fitted correlation lengths

This appendix presents further details of the statistical analysis reported in Bale et al. (2011).

Correlation lengths are determined by the following steps. The correlation $C_{\xi}^{(\alpha)}$ for the deviation $\xi=x$, y, or z of tow type $\alpha=w$, tw, cw, or bw is computed as a function of the separation k of pairs of grid points on the same tow. All available data from a single tow are obtained by varying the grid pair (k_1, k_2) subject to $k_2-k_1=k$. The data from different tows are then collated into a single set, from which the function $C_{\xi}^{(\alpha)}(k)$ is computed. The correlation length, ζ, is determined by fitting a straight line $C=1-k\delta/\zeta$ to the function $C_{\xi}^{(\alpha)}(k)$ over the domain of small k, which is chosen to be the domain where $C_{\xi}^{(\alpha)}(k)$ trends down towards zero.

The effect of sample size on the uncertainty resulting from this fitting procedure is illustrated for the subject carbon/SiC composite of this paper by the data plots of Fig. A1. The function $C_{\xi}^{(\alpha)}(k)$ for individual tows (Fig. A1a and c) shows substantial variability due to the fact that the length of individual tows in a μCT specimen is only a small multiple of the correlation length. Therefore, the deviations of a single tow may not even be indicative of the deviations of a large ensemble. In particular, the slope of the function $C_{\xi}^{(\alpha)}(k)$ near $k=0$ can vary substantially.

The statistics of correlations are much better established when all the data from tows of the same genus are collated (Fig. A1b and d). Using the available data for the carbon/SiC composite, a reasonable estimate of the uncertainty in the correlation length for any deviation component on any tow genus is approximately $\pm 25\%$, with the distribution of deduced correlation lengths skewed to include a significant frequency of large values.

While the available data show larger uncertainty in correlation lengths for particular deviations on particular tows (e.g., the correlation lengths for center weft tows show more scatter than those for warp tows in Fig. A1), there is no *a priori* reason to expect greater fractional uncertainty for one tow type. Therefore, the uncertainty $\pm 25\%$ is regarded as representative of all deviations on all tow genuses.

The substantial uncertainty in the correlation lengths deduced from μCT data should be allowed for when assessing whether the statistics of generated virtual specimens are consistent with experiment.

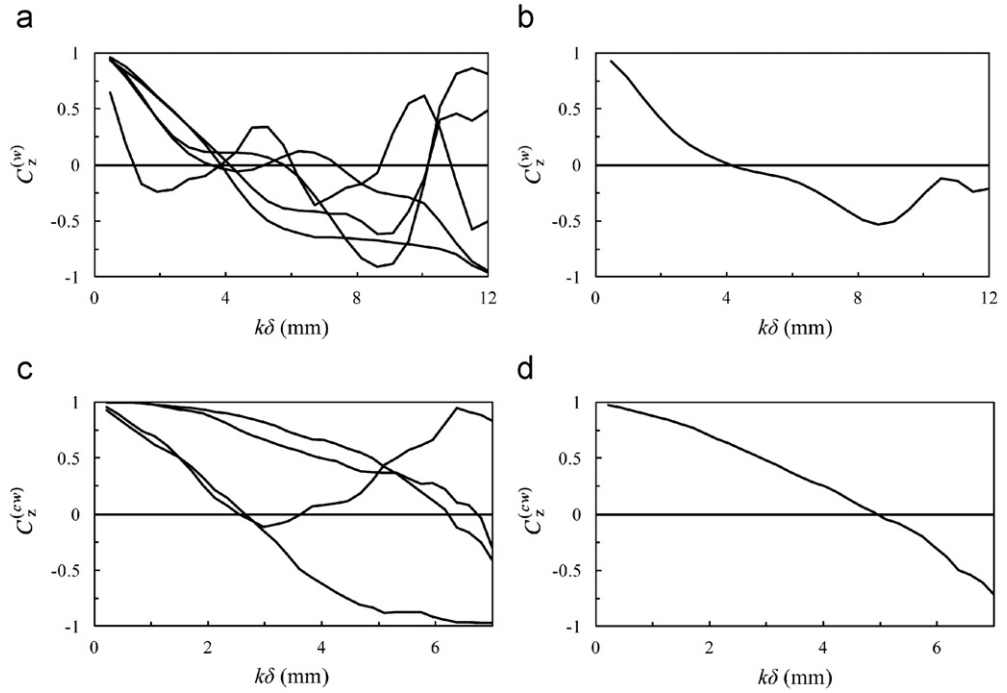

Fig. A1. Data for the correlation between deviations in the z-direction as a function of the distance $k\delta$ between two points on the same tow: (a) plots for individual warp tows, (b) plots for the data in (a) collated into a single set, (c) and (d) the same plots for center weft tows. Data for a carbon fiber/SiC matrix composite.

Appendix B. Smoothing and interpolating procedures that conserve the RMSD

B.1. Smoothing

Smoothing is effected by a variant of the moving average or moving-box procedure. The standard moving average is defined by

$$x_i^{(s)} = \frac{1}{2m+1} \sum_{j=-m}^{m} x_{i+j} \tag{B.1}$$

where the superscript s denotes a smoothed quantity. If x_i is distributed around zero (as in the cases that x represents a deviation), then the RMSD of x_i is defined by

$$\sigma_x = \sqrt{\sum_i x_i^2/N} \tag{B.2}$$

where N is the number of grid points. When Eq (B.2) is applied to the set of smoothed quantities $x_i^{(s)}$, the result is not the same as the RMSD of the original quantities x_i.

Therefore consider instead the smoothing operation

$$x_i^{(s)} = S\sqrt{\frac{1}{2m+1} \sum_{j=-m}^{m} x_{i+j}^2} \tag{B.3}$$

where $S = \pm 1$ is a sign factor and the result of taking the square root is a non-negative number. Rule (B.3) is only applied where all x_{i+j} in the averaging interval have the same sign or are zero. The sign of the non-zero terms becomes the sign of S. The rule is not applied where the sequence x_i crosses $x=0$ in the averaging interval. For intervals containing sign changes in x_i, the conventional averaging rule of Eq. (B.1) is used.

It is easily seen that Eq. (B.3) tends to conserve the RMSD: when evaluating Eq. (B.2) for the smoothed quantities, each of the original quantities will appear in the sum of squares $2m+1$ times, canceling the factor $2m+1$ in Eq. (B.3) and one recovers Eq. (B.2) as it stood for the original quantities. Therefore, the smoothing rule of Eq. (B.3) preserves the RMSD exactly in cases where the sequence x_i contains no passages through zero and does so very well when passages through zero are present occasionally. Passages through zero are relatively infrequent in the deviations generated by the Markov chain algorithm, because the grid is dense compared to the correlation length for deviations; and the contribution of elements near a zero to the RMSD is small anyway, because they are near zero.

In applying Eq. (B.3), attractive results are found by choosing $m=1$ and then repeating the application of Eq. (B.3) recursively. This creates an averaging that concentrates weight around the central element. The results presented in the paper were obtained with four recursions of Eq. (B.3).

B.1. Interpolation

In cases where strong correlation exists between warp and weft deviations, the complete set of deviations for one tow genus is formed by interpolating between the values generated at the cross-overs where the inter-tow correlation is taken into account (Section 3.4). A method of interpolation can be devised that preserves the RMSD of the deviations, i.e., generates a complete set of deviations that has the same RMSD as the deviations prescribed at cross-overs.

Consider the problem of interpolating between two points, which without loss of generality will be taken to be 0 and X. Let the function to be interpolated have the values f_0 and f_1 at these points.

If f_0 and f_1 have the same sign, define an interpolating function by

$$f(x)=\sqrt{\frac{x}{X}f_1^2+\frac{X-x}{X}f_0^2}. \tag{B.4}$$

Considering $f(x)$ to be a continuous random function, the contribution to its mean square deviation arising from the interval $0\le x\le X$ is

$$\sigma_f=\frac{1}{X}\int_0^X f^2\,dx=\frac{1}{2}f_0^2+\frac{1}{2}f_1^2 \tag{B.5}$$

If f_0 and f_1 have different sign, define an interpolating function by

$$r=\frac{f_0}{f_0-f_1}X \tag{B.6a}$$

$$f(x)=\sqrt{\frac{r-x}{r}}f_0 \quad (x\le r) \tag{B.6b}$$

$$f(x)=\sqrt{\frac{x-r}{X-r}}f_1 \quad (x>r) \tag{B.6c}$$

Continuing to consider $f(x)$ a continuous random function, the contributions to its mean square deviation arising from the intervals $0\le x\le r$ and $r<x\le X$ are

$$\sigma_{\mathrm{f}}=\frac{1}{r}\int_0^r f^2\,dx=\frac{1}{2}f_0^2 \tag{B.7a}$$

and

$$\sigma_{\mathrm{f}}=\frac{1}{(X-r)}\int_r^X f^2\,dx=\frac{1}{2}f_1^2 \tag{B.7b}$$

respectively.

Combining the contributions to σ_f from all intervals of length X_i in a long sequence spanning N grid points, one finds from Eqs. (B.5) and (B.7) that

$$\sigma_f=\frac{1}{\sum_{i=1}^N X_i}\int f^2\,dx=\sum_{i=1}^N f_i^2 \tag{B.8}$$

and thus the RMSD is preserved by the interpolation.

References

Argon, A.S., 1972. Fracture of Composites. Academic Press, New York.

Ashby, M.F., 1992. Physical modelling of materials problems. Materials Science and Technology 8, 102–111.

Bale, H., Blacklock, M., Begley, M.R., Ritchie, R.O., Marshall, D.B., Cox, B.N. Characterizing three-dimensional textile ceramic composites using synchrotron X-ray micro-computed-tomography. Journal of the American Ceramic Society, doi:10.1111/j.1551-2916.2011.04802.x, in press.

Budiansky, B., 1983. Micromechanics. Composite Structures 16 (1), 3–12.

Cox, B.N., 1989. Inductions from Monte Carlo simulations of small fatigue cracks. Engineering Fracture Mechanics 33, 655–670.

Cox, B.N., Carter, W.C., Fleck, N.A., 1994. A Binary Model of textile composites: I Formulation. Acta Metallurgica et Materialia 42, 3463–3479.

Cox, B.N., Dadkhah, M.S., 1995. The macroscopic elasticity of 3D woven composites. Journal of Composite Materials 29 (6), 785–819.

Cox, B.N., Morris, W.L., 1987a. Model-based statistical analysis of short fatigue crack growth in Ti 6Al-4Sn-2Zr-6Mo. Fatigue and Fracture of Engineering Materials and Structures 10, 429–446.

Cox, B.N., Morris, W.L., 1987b. A probabilistic model of short fatigue crack growth. Fatigue and Fracture of Engineering Materials and Structures 10, 419–428.

Cox, B.N., Morris, W.L., 1988. Monte Carlo simulations of the growth of small fatigue cracks. Engineering Fracture Mechanics 31, 591–610.

Cox, B.N., Spearing, S.M., Mumm, D.R., 2008. Practical challenges in formulating virtual tests for structural composites. In: Camanho, P.P., Dávila, C.G., Pinho, S.T., Remmers, J.J.C. (Eds.), Mechanical Response of Composites, vol. 10. , Springer Science and Business Media, Dordrecht, pp. 57–75.

Cox, B.N., Yang, Q.D., 2006. In quest of virtual tests for structural composites. Science 314, 1102–1107.
Dadkhah, M.S., Flintoff, J.G., Kniveton, T., Cox, B.N., 1995a. Simple models for triaxially braided composites. Composites 26, 91–102.
Dadkhah, M.S., Morris, W.L., Cox, B.N., 1995b. Compression-compression fatigue in 3D woven composites. Acta Metallurgica et Materialia 43 (12), 4235–4245.
Desplentere, F., Lomov, S.V., Woerdeman, D.L., Verpoest, I., Wevers, M., Bogdanovich, A.E., 2005. Micro-CT characterization of variability in 3D textile architecture. Composite Science and Technology 65, 1920–1930.
Fleck, N.A., Budiansky, B., 1991. Compressive failure of fibre composites due to microbuckling. In: Dvorak, G.J. (Ed.), Inelastic Deformation of Composite Materials, Springer-Verlag, New York, pp. 235–274.
Fleck, N.A., Shu, J.Y., 1995. Microbuckle initiation in fibre composites: a finite element study. Journal of the Mechanics and Physics of Solids 43 (12), 1887–1918.
Frobenius, G., 1912. Ueber Matrizen aus nicht negativen Elementen. Sitzungsber. Konigl. Preuss. Akad. Wiss, 456–477.
Groeber, M., Ghosh, S., Uchic, M.D., Dimiduk, D.M., 2008. A framework for automated analysis and simulation of 3D polycrystalline microstructures. Part 2: Synthetic structure generation. Acta Materialia 56, 1274–1287.
Hillig, W.B., 1994. Effect of fibre misalignment on the fracture behaviour of fibre-reinforced composites. Part I. Experimental. Journal of Materials Science 29, 419–423.
Jiao, Y., Stillinger, F.H., Torquato, S., 2009. A superior descriptor of random textures and its predictive capacity. Proceedings of the National Academy of Science of the USA 106 (42), 17634–17639.
Pastore, C.M., 1993. Quantification of processing artifacts in textile composites. Composites Manufacturing 4 (4), 217–226.
Perron, O., 1907. Zur Theorie der Matrices. Mathematische Annalen 64 (2), 248–263.
Pollock, T.M., Allison, J.E., Backman, D.G., Boyce, M.C., Gersh, M., Holm, E.A., LeSar, R., Long, M., Powell Jr., A.C., Schirra, J.J., Whitis, D.D., Woodward, C., 2008. Integrated computational materials engineering: a transformational discipline for improved competitiveness and national security. National Research Council of the National Academies, Washington, D.C.
Rosen, B.W., 1965. Mechanics of composite strengthening. Fiber Composite Materials. American Society of Metals, Metals Park, Ohio: pp. 35-75.
Xu, J., Cox, B.N., McGlockton, M.A., Carter, W.C., 1995. A Binary Model of textile composites: II Elastic regime. Acta Metallurgica et Materialia 43, 3511–3524.
Yang, Q., Cox, B.N., 2010. Predicting failure in textile composites using the Binary Model with gauge averaging. Engineering Fracture Mechanics 77, 3174–3189.
Yang, Q.D., Cox, B.N., 2003. Spatially averaged local strains in textile composites via the Binary Model formulation. Journal of Engineering Materials and Technology 125, 418–425.
Yurgatis, S.W., 1987. Measurement of small angle fiber misalignments in continuous fiber composites. Composites Science and Technology 30, 279–293.
Yushanov, S.P., Bogdanovich, A.E., 2000. Fiber waviness in textile composites and its stochastic modeling. Mechanics of Composite Materials 36 (4), 297–318.